Effect of Electron Beam Oscillation Welding of Molybdenum and Titanium

The microstructure, element distribution, chemical composition, microhardness, and tensile strength of the welded joints were analyzed

BY X.-M. SHI, D.-F. MO, T. ZHAO, Y. ZHANG, W. SUN, H. GONG, AND X. LI

Abstract

Electron beam welding of pure molybdenum (Mo) and titanium alloy (Ti-6Al-4V) was performed with beam oscillation. The effects of beam oscillation with offset on the welded joints were analyzed in terms of microstructure, element distribution, chemical composition, microhardness, and tensile strength. The results showed that the fusion zone expanded with beam oscillation. Reaction layers were generated in both joints welded with and without beam oscillation. The thickness of the reaction layers decreased along the perpendicular direction. The reaction layers were (Mo, Ti) solid solutions. Both welded joints consisted of single-phase Mo, the β-Ti phase, and Mo-Ti solid solutions. The microhardness distribution of the joint welded with beam oscillation was more consistent than that of the joint welded without beam oscillation, and the maximum hardness was reduced from 340 HV to 270 HV. The tensile strength increased from 124 MPa to 204 MPa.

Keywords

- Electron Beam Welding
- Titanium Alloy
- Molybdenum
- Microstructure

Introduction

Titanium (Ti) alloys are widely used in the nuclear and aerospace fields due to their low density, low heat conductivity, and excellent mechanical qualities (Ref. 1). Molybdenum (Mo) and its alloys are commonly applied in facilities such as nuclear power plants because of their extraordinarily high thermal conductivity and melting points (Refs. 2, 3). In the low-temperature packaging field, extreme thermal conductivity is required to reduce the detector to a lower temperature with limited cooling resources to achieve higher detection. Mo is widely used as a cold platform (Ref. 4) for inserting detector chips due to its exceptional low-temperature thermal conductivity and excellent coefficient of thermal expansion, which is similar to that of the chips. Ti alloy is used as a support (Ref. 5) to connect the cold platform to the cooler. Moreover, the extremely low thermal conductivity of Ti minimizes heat loss. As a result, realizing the welding of these two dissimilar metals and increasing their joint performance are worth investigating.

Many researchers have studied the welding of pure Mo and Mo alloys. Chen et al. (Ref. 6) found many holes and crystal cracks in the weld zone of Mo joints produced by electron beam welding. The research results showed that the pores were caused by oxygen not escaping in time. Ambroziak (Ref. 7) investigated friction welding of Mo and dissimilar metals such as vanadium (V), tantalum (Ta), nickel (Ni), Mo, and copper (Cu). The research results showed that refractory metals could be successfully welded through friction welding with no intermetallic phases in the welded joints. Zhang, L.-J. et al. (Ref. 8) successfully connected pure Mo to pure Ti by laser welding with beam offset. The highest tensile strength was 346 MPa when the beam offset was 0.5 mm (0.019 in.) from the splice site. Zhou et al. (Ref. 9) used Ti-6Al-4V and Ni as interlayers to achieve laser welding of Mo and Ta. The result showed that a reaction layer composed of the β-Ti phase was formed at the interface. Although there has been much research on dissimilar metal connections for molybdenum and researchers performed laser welding of molybdenum on titanium alloy, Ti alloy welding is extremely sensitive to welding atmosphere. Thus, electron beam welding with a vacuum environment has obvious advantages.

In the process of improving the appearance and properties of welded joints, welding with beam oscillation was introduced. Zhou et al.(Ref. 9) proved that increasing laser beam oscillation during welding accelerated the formation of equiaxed dendritic grains and reduced the risk of hot

https://doi.org/10.29391/2024.103.003

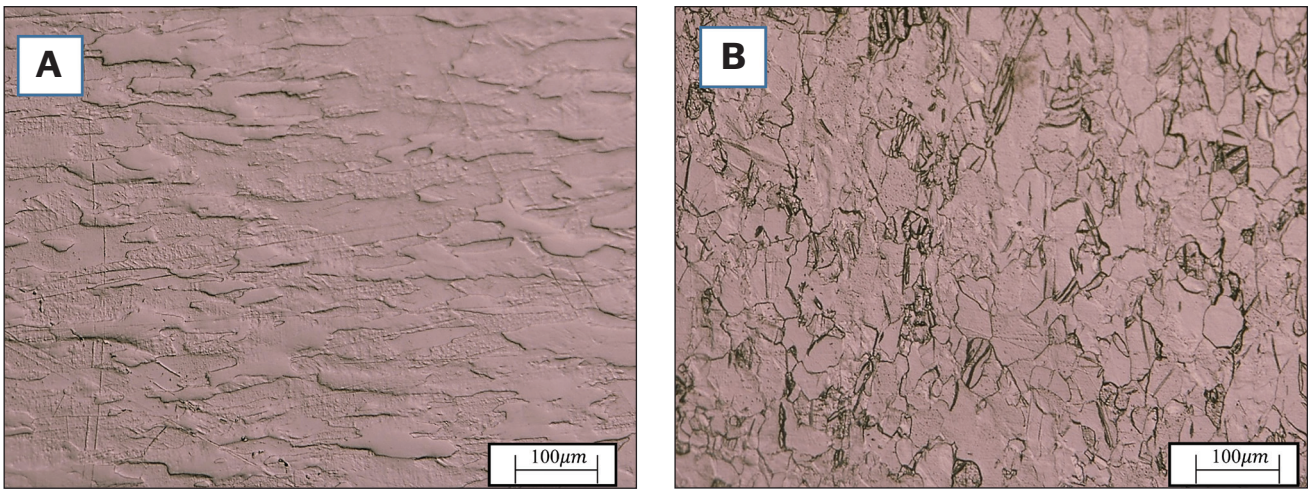

Fig. 1 — Microstructures of base metals: A — Mo; B — Ti-6Al-4V.

Table 1 — The Physical Properties of the Base Metals

Alloy	Density ($g \cdot cm^{-3}$)	Melting Point (°C)	Thermal Conductivity (W/m·K)	CTE (10^{-6} K^{-1})	Tensile Strength (25°C) (MPa)
Mo	10.2	2620	142.35	5.3	742
TC4	4.55	1725	7.5	7.1	978

Table 2 — Welding Parameters Used in This Experiment

Sample	Accelerating Voltage (kV)	Beam Current (mA)	Welding Speed (mm/s)	Oscillation Frequency (Hz)	Offset (mm)	Heat Input (J/mm)
1	55	14	5	Not used	+0.2	154
2	55	14	5	50	+0.2	12.27

Table 3 — Chemical Composition of the Base Metals (wt-%)

Alloy	Mn	Si	C	Fe	Co	Ni	Ti	Al	V	N	H	O	Mo
Mo	—	0.01	0.02	0.005	—	0.002	—	0.002	—	—	—	—	bal.
TC4	—	0.15	0.1	0.3	—	—	bal.	6	4	0.05	0.015	0.2	—

cracks. Yan et al. (Ref. 10) studied the effect of laser beam oscillation welding on the joint of copper and stainless steel. It was found that a vortex flow was formed in the molten pool with beam oscillation, which enhanced heat and mass transfer in the weld pool and increased the tensile strength by 110% compared to that without oscillations. Jiang et al. (Ref. 11) compared the effect of laser oscillation welding on Ni-Cr-Mo and Cu-Cr-Zr joints. The tensile strength of the joints welded with beam oscillation increased by 20% because of the impact of solid solution strengthening. The effect of electron beam oscillation on joints of dual-phase steel and 5754 aluminum alloy was studied by Dinda (Ref. 12). The oscillating beam joint demonstrated 70% higher elongation than the nonoscillating beam counterpart.

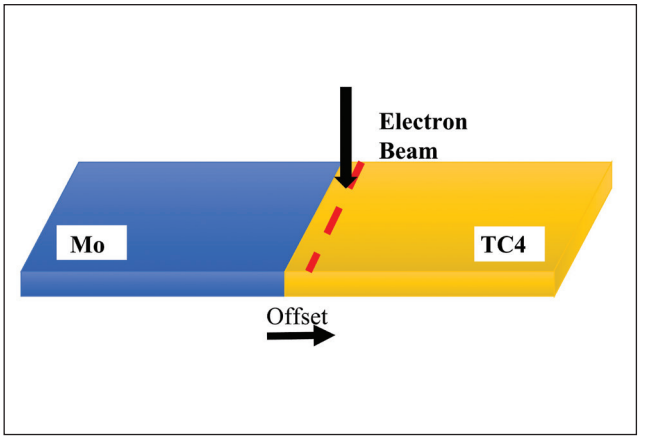

Fig. 2 — Schematic diagram illustrating electron beam welding Mo/TC4 with offset.

Despite extensive studies, electron beam welding of pure Mo and Ti alloys and the effect of oscillation welding on welded joints have not yet been reported. Electron beam welding has a more focused energy than laser welding, giving it an advantage for welding refractory metals. As a result, electron beam welding is employed in this study. Electron beam oscillation welding is used to increase the performance of the welded joints. The influence of electron beam oscillation welding on the morphology, microstructure, and mechanical properties is also investigated.

Experimental

Materials and Preparation

The base metals in this paper were pure Mo and TC4 alloys, which were machined in 50 mm (1.968 in.) × 30 mm (1.181 in.) × 2 mm (0.079 in.) plates. The physical parameters of Mo and TC4 are shown in Table 1. The chemical composition of the base metals are shown in Table 2. The microstructures of the two materials are displayed in Fig. 1. As illustrated in Fig. 2, the electron beam was applied to the TC4 base material with a 0.2 mm (0.008 in.) offset from the joint line. The parameters are listed in Table 3. The oscillation patterns used were circular. The heat input of the parameters without and with oscillation were 154 J/mm and 12.27 J/mm, respectively. Sample 1 corresponded to non-oscillation welding parameters, whereas Sample 2 corresponded to electron beam oscillation welding parameters with a circular oscillation waveform.

Analytical Methods

Pure Mo and Ti alloys were degreased and cleaned with alcohol before welding. The Mo part was etched by an acid mixture (nitric acid: hydrofluoric acid: water = 5:2:3 by volume), and the TC4 alloy part was etched by another acid mixture (nitric acid: hydrofluoric acid: water = 1:1:4 by volume). The cross-sections and microstructures of the welded joints were observed by optical microscopy and scanning electron microscopy (SEM) using the ZEISS Sigma 300. Moreover,

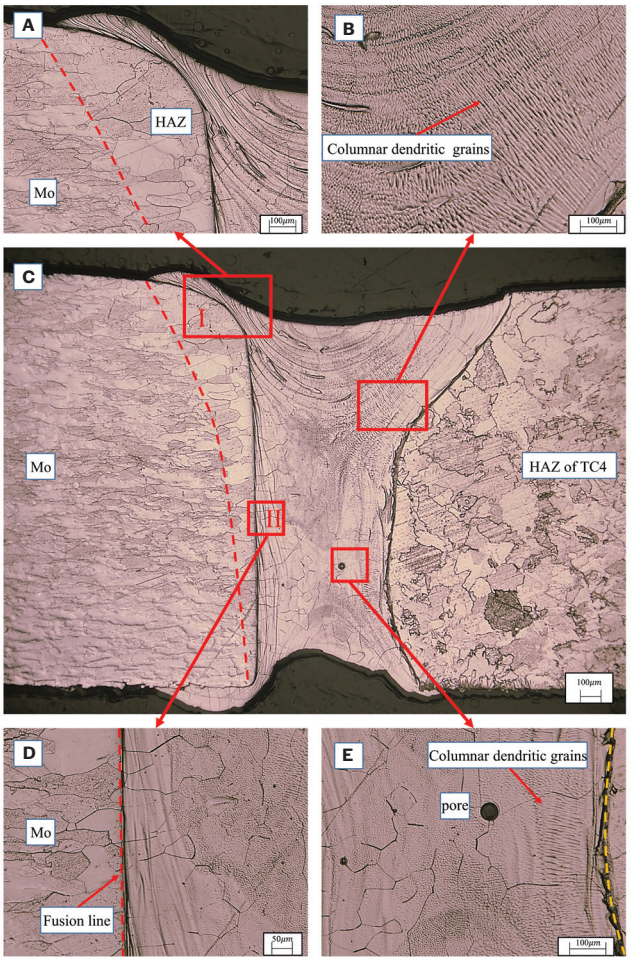

Fig. 3 — Cross-section morphology of the joint without beam oscillation: A — Mo side; B — TC4 side; C — total morphology; D — lower Mo side; E — lower weld zone.

the element composition was analyzed through SEM-energy-dispersive x-ray spectroscopy (EDS) in spot mode. The phase composition of the welded joints was identified by x-ray diffraction (XRD) using the Panalytical-Empyrean diffractometer. The acceleration voltage of the XRD equipment was 40kV, the operating current was 40mA, and the scanning range was 20 deg–90 deg (2θ) at the scanning speed of 2 deg/min^{-1}. The microhardness of the welded joints was tested by an HXD-100TM/LCD microhardness tester under 100 g (0.220 lb) continuous compression for 15 s, and three tensile strength samples were prepared for each parameter. The tensile strength of the joints was measured by a WDW-310 material testing machine at a constant rate of 0.5 mm/min. The fracture morphology was observed through SEM.

Results and Discussion

Weld Appearance

Figure 3 shows the cross-sectional morphology of the Mo and TC4 joints welded without beam oscillation. The non-symmetrical weld zone is shown in Fig. 3C. The fusion line

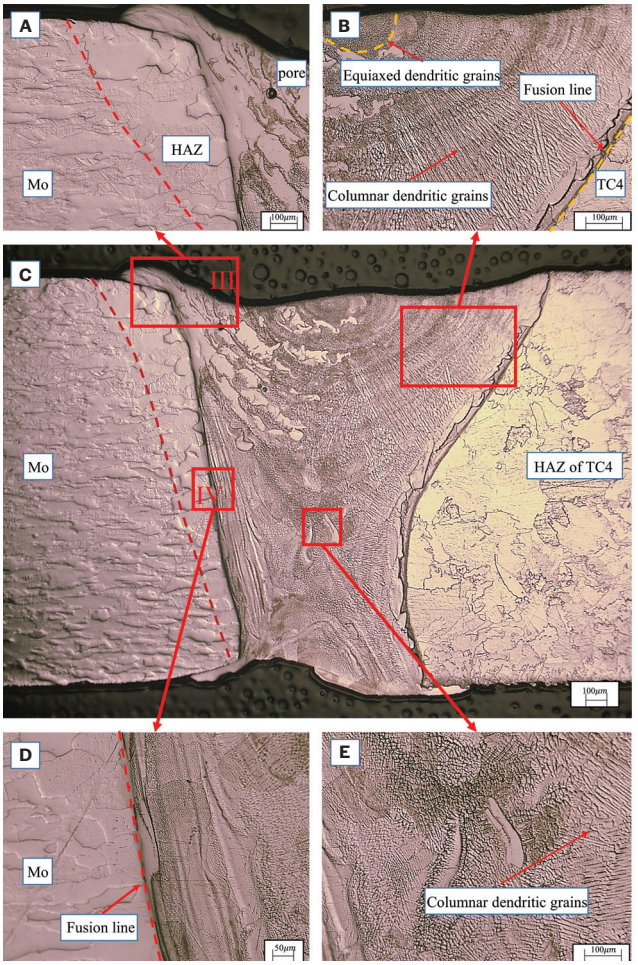

Fig. 4 — Cross-section morphology of the joint with beam oscillation: A — Mo side; B — TC4 side; C — total morphology; D — lower Mo side; E — lower weld zone.

on the Mo side is straight, whereas the fusion line on the TC4 side is nearly conically shaped. Weld metal overlays are observed on the top and bottom surfaces of the Mo base metal, which is related to the excellent wettability of liquid TC4 on Mo. The heat-affected zone (HAZ) becomes narrower on the Mo side, which is consistent with the characteristics of the input heat source, and recrystallization occurs in this area. A lattice can be observed in the weld zone in Fig. 3D. As shown in Figs. 3B and E, there are pores in the weld zone caused by the untimely escape of gases during welding. The weld zone exhibits columnar dendritic grains along the fusion line on the TC4 side, and these grains extend into the interior of the weld zone. The weld root size (0.68 mm [0.026 in.]) is two-fifths of the weld zone's top size (1.6 mm[0.063 in.]).

Figure 4 shows the cross-sectional morphology of the joint welded with beam oscillation. Fig. 4C shows that the fusion line on the Mo side is obliquely shaped, and the fusion line on the TC4 side is nearly conically shaped. Due to the deeper melting of the Mo base metal, the fusion line on the Mo side changed from straight to oblique. The microstructure of the weld zone was different from that produced without beam oscillation. Molten Mo increased due to beam oscillation.

Table 4 — Main Chemical Constituents (at-%) in Different Points

Point	Mo	Ti	V	Al
A	97.00	1.76	0.70	0.54
B	39.82	56.59	2.84	0.39
C	24.59	72.51	2.59	0.31
D	13.89	83.80	2.08	0.24
E	9.05	88.82	1.97	0.15
F	74.37	23.55	1.60	0.48
G	20.73	77.01	2.04	0.22
H	14.24	83.76	1.97	0.04
!	11.25	87	1.70	0.05

Some molten Mo entered the weld zone, while significant continuous white phases gathered on the upper part of the fusion line on the Mo side (Refs. 13–15). A minor quantity of white phases is generated on the fusion line, as seen in Figs. 4C and D. These white phases consisted of a Mo-Ti solid solution with high molybdenum element content. They have a high melting point, so the white phase formed first in the weld zone. There was a small amount of equiaxed dendritic grains in the center of the weld zone. Beam oscillation is inferred to exert a substantial effect on the weld zone. Therefore, columnar dendritic grains were broken and transformed into equiaxed dendritic grains. The weld zone expanded because of the oscillation, and the weld root size was 0.68 mm (0.027), while the weld zone top size was 1.8 mm (0.071 in.).

Microstructures of the Joints

Microstructures of the Mo-side Interface Produced without Beam Oscillation

Figure 5A shows the microstructure of Zone I located at the upper fusion line in Fig. 3C. There was a neat and flat reaction layer between the Mo base metal and weld zone. Figs. 5B and C show the element distribution in Zone I. Mo and Ti were dispersed with the fusion line as the boundary. Furthermore, the line scanning result of the selected area is shown in Fig. 5D. Mo precipitously declined at the interface and diffused into the weld zone. However, Ti was nearly nonexistent in the Mo base metal after passing through the reaction layer. The average thickness of the reaction layer was approximately 2 μm.

Figure 6 shows the analysis result of Zone II located at the lower fusion line in Fig. 3C. A similar element distribution to that in Fig. 5 can be seen in Fig. 6, but the most significant difference was that the Ti element diffused into the Mo base

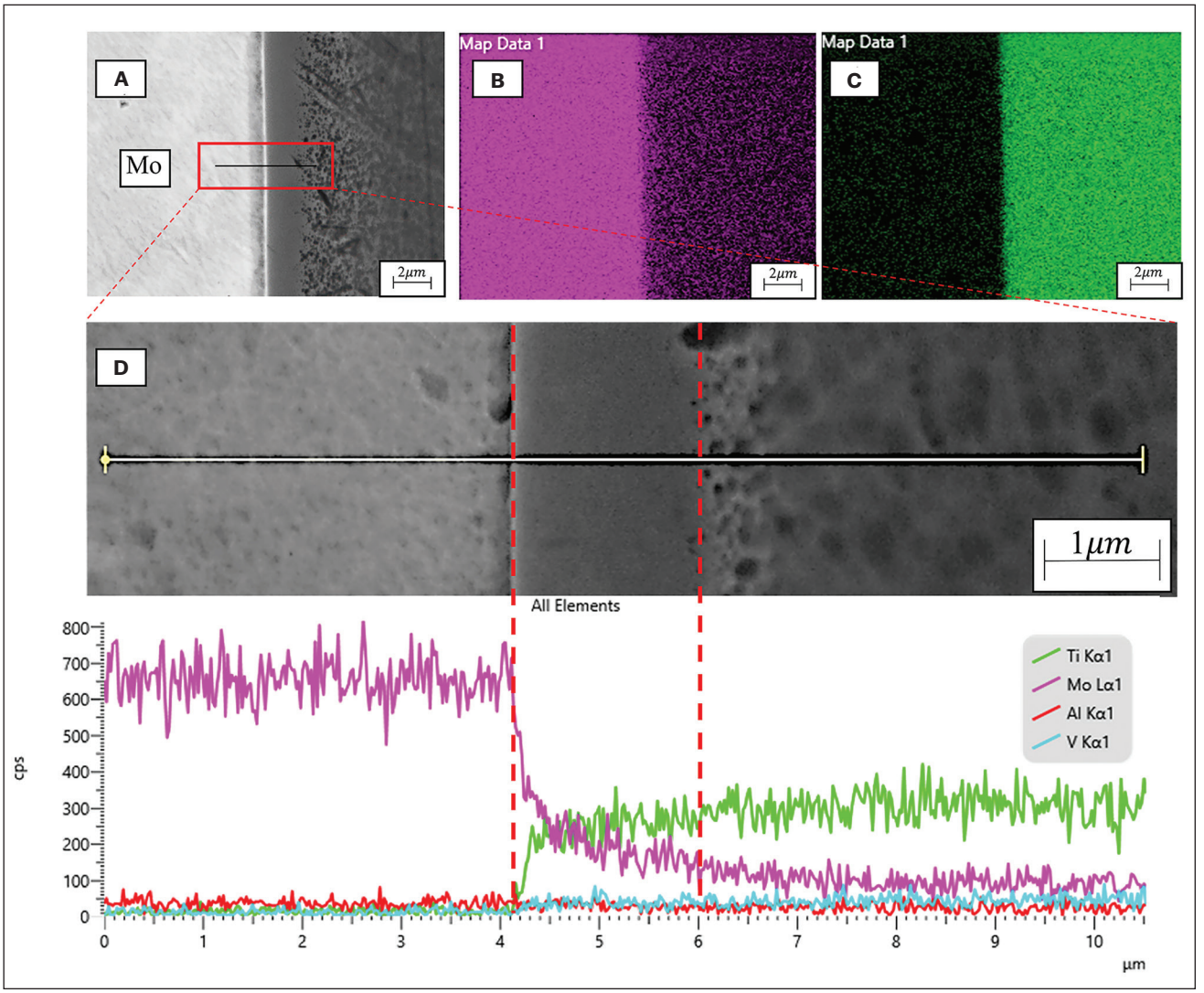

Fig. 5 — Microstructures of the upper interface without beam oscillation: A — SEM micrograph; B — map scanning result of element Mo; C — map scanning result of element Ti; D — line scanning results.

metal. Meanwhile, the thickness of the reaction layer was thinner than that in Zone I.

Furthermore, a mathematical model of Mo diffusion as a function of the local temperature was applied (Ref. 16). The concentration gradient of Mo at the solid-liquid interface was used to calculate Mo diffusion, and the formula for the thickness of the reaction layer was determined to be as follows (Ref. 17).

$$\Delta z = \int_{t_0}^{t_L} V_c \, dt = \int_{t_0}^{t_L} D \left(\frac{\partial C}{\partial y} \right) dt \qquad (1)$$

where D is the temperature-dependent diffusion coefficient, C is the Mo concentration, t_0 is the moment when the solid state comes in contact with the liquid state, and t_L is the time to form a solid solution. Several factors contributed to a decreasing thickness of the reaction layer. First, the local temperature of Zone I was higher than that of Zone II, which was related to the decrease in the heat input in the perpendicular direction as a result of the difference in the diffusion coefficient. Second, different locations were exposed to liquid TC4 at different times. Zone I exposure occurred earlier than Zone II exposure. A similar phenomenon was found for the Mo-Ti reaction layer by Luo et al. (Ref. 18).

Microstructures of the Mo-side Interface Produced with Beam Oscillation

To analyze the effect of beam oscillation on welded joints, the microstructure of the weld zone was analyzed. The microstructures of Zones III and IV in Fig. 4C are shown in Figs. 7A and B, respectively. Fig. 7A shows that there was no reaction layer in the upper weld zone. The line scanning result revealed that the Mo and Ti contents varied drastically at the inter-

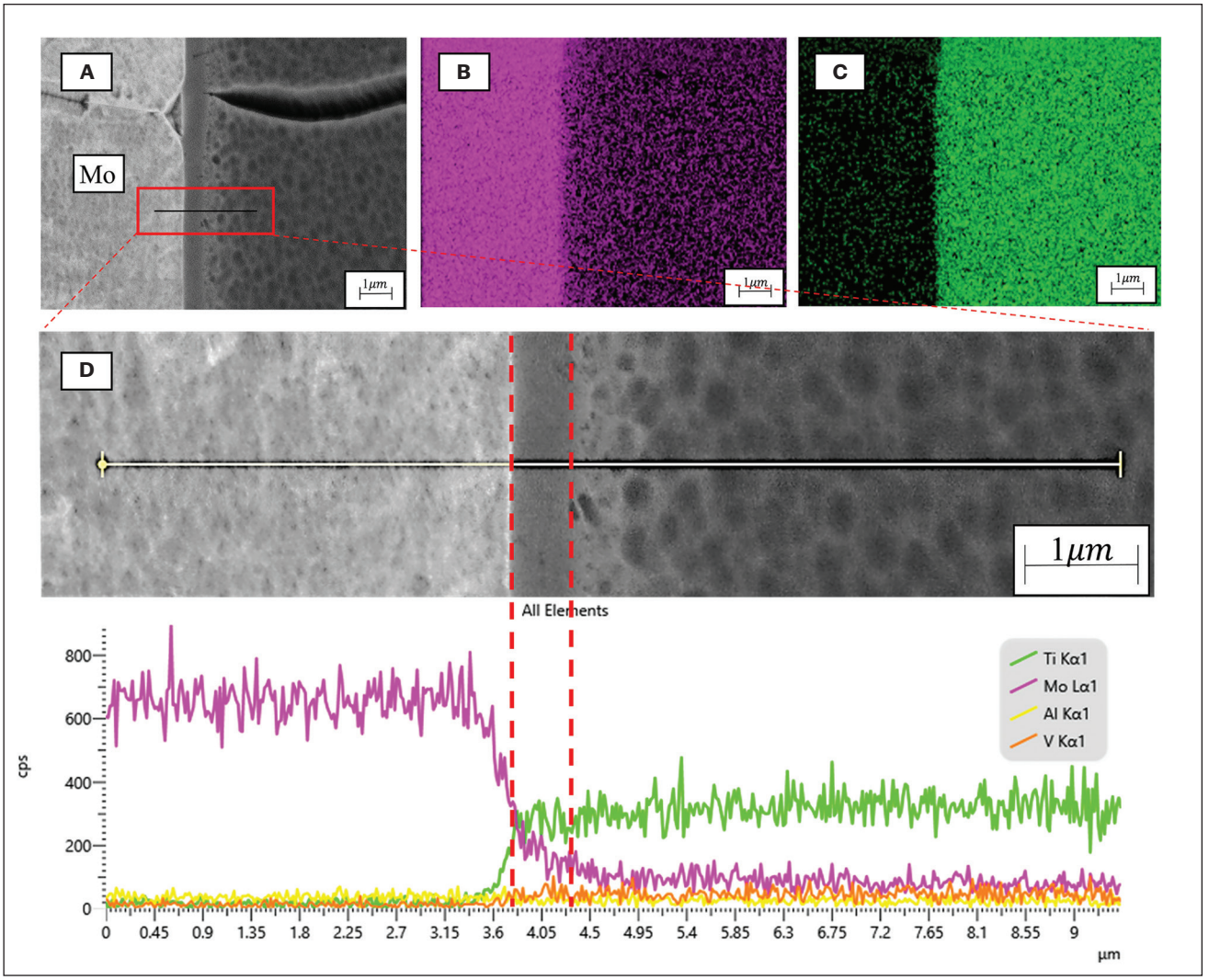

Fig. 6 — Microstructures of the lower interface without beam oscillation: A — SEM micrograph; B — map scanning result of element Mo; C — map scanning result of element Ti; D — line scanning results.

face and that volatility was generated as a result of beam oscillation. As shown in Fig. 7B, there was a smooth and flat reaction layer in the lower weld zone, and the layer thickness decreased. The Mo and Ti distributions were stable in this weld zone according to the line scanning result.

Compared with the microstructure of the interface produced without beam oscillation, there was no reaction layer in Zone III, while the thickness of the reaction layer in Zone IV was greater than that in Zones I and II. When the oscillation was activated, the keyhole migrated to the Mo base metal. The initial boundary of the Mo base metal melted, and liquid Mo entered the melt pool and mixed with the liquid Ti to generate a solid solution. As shown in Fig. 7B, the lack of mixing of molten Mo with liquid Ti caused the formation of a reaction layer in Zone IV.

To identify the chemical compositions of the phases marked in Figs. 7A and B, the compositions were measured by EDS, as shown in Table 4. According to the binary phase diagram of Mo-Ti (Ref. 19), all the selected points mainly consisted of the Mo-Ti solid solution. The difference was that the Mo content decreased at the points away from the interface. Point EDS analysis of both joints was carried out, as shown in Fig. 8. The Mo content of the points in the weld zone produced without beam oscillation was approximately 6%, while that of the points in the weld zone produced with beam oscillation was approximately 12%. Beam oscillation caused enhancement of molten Mo. As a result, the Mo content in the weld zone increased. The XRD results are shown in Fig. 9. The weld zone of both joints consisted of a single phase Mo, the β-Ti phase, and a Mo-Ti solid solution. This was consistent with the previous analysis.

Mechanical Properties of Welded Joints

Microhardness Analysis of Welded Joints

The microhardness of the upper, middle, and bottom parts of the joints welded with and without beam oscillation were

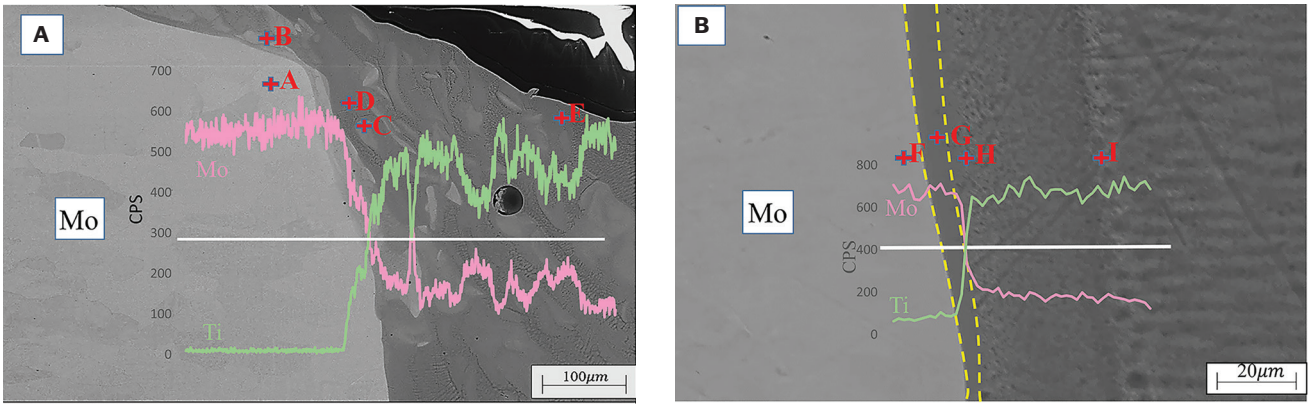

Fig. 7 — Microstructures of interface with beam oscillation: A — Upper interface; B — lower interface.

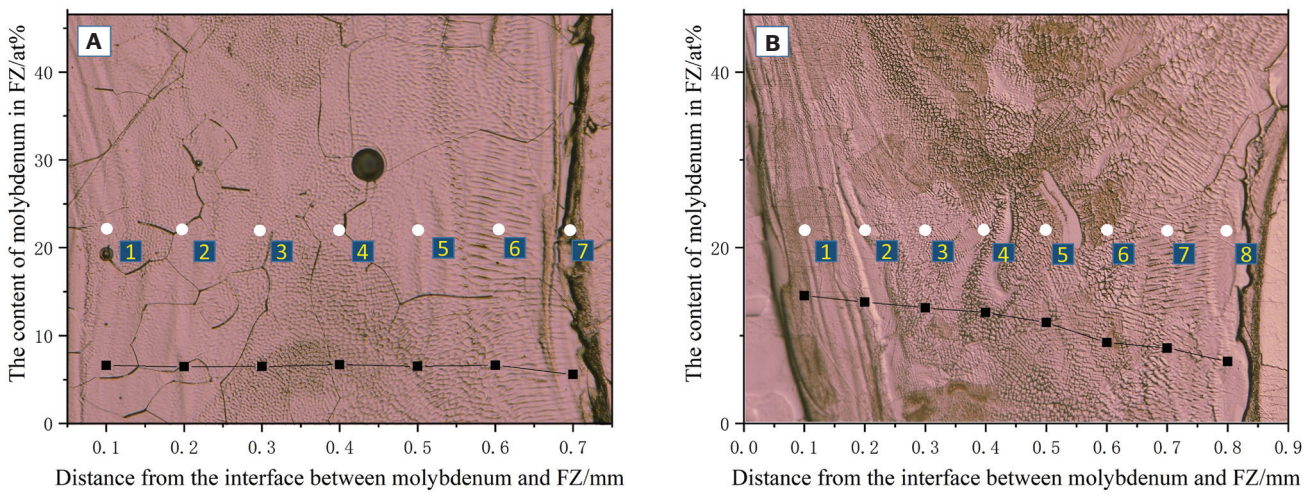

Fig. 8 — EDS result of content of molybdenum in weld zone: A — Without beam oscillation; B — with beam oscillation.

tested. The results are shown in Fig. 10. The hardness values of the Mo and TC4 alloys were 230 HV and 160 HV, respectively. Fig. 10B shows the hardness of the joint welded without beam oscillation. Due to recrystallization, the microhardness of the HAZ on the Mo side was lower than that of the Mo base metal. The weld zone exhibited a higher hardness than in the base metals.

Moreover, the hardness of the bottom part of the welded joint was higher than that of the upper part. Maximum hardness of 340 HV was measured, located in the bottom part of the weld zone. This result was related to the difference in the local cooling rate after welding. Fig. 10D shows the hardness of the joint welded with beam oscillation. The most significant difference was that the hardness of the weld zone was much more uniform, and the value was approximately 260 HV. A maximum hardness of 280 HV was measured, located in Mo-rich phases near the fusion line on the Mo side. Due to beam oscillation, the Mo content in the weld zone was higher as a result of an increase in molten Mo. According to the investigation of Ho et al. (Ref. 20), the microhardness of Mo-Ti alloys decreases with increasing Mo content. For these reasons, the microhardness of the weld zone decreased.

Tensile Strength and Fracture of Welded Joints

A tensile strength test was carried out. The average tensile strength of the joint welded without beam oscillation was 124 MPa, which was only 17% of the value of Mo and 13% of the value of TC4. The average tensile strength of the joint welded with beam oscillation was 204 MPa, representing an increase of 64% compared to that without beam oscillation. The fracture surfaces of the joints welded with and without beam oscillation are shown in Fig. 11. The fracture surface of the joint welded without beam oscillation on the weld side consisted of reflective faces, indicating intergranular fracture, as shown in Fig. 11A. There were grains surrounded by cavities at the bottom of the fracture surface, indicating a decrease in joint strength. Fig. 11B shows the fracture surface with

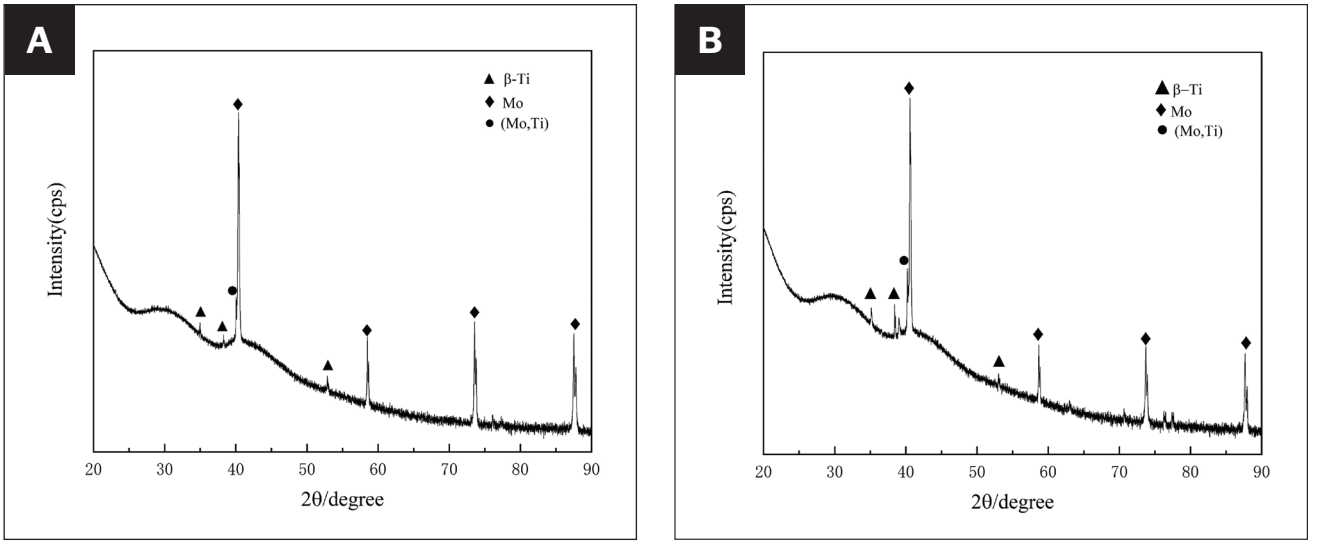

Fig. 9 — XRD analysis of the weld zone: A — Without beam oscillation; B — with beam oscillation.

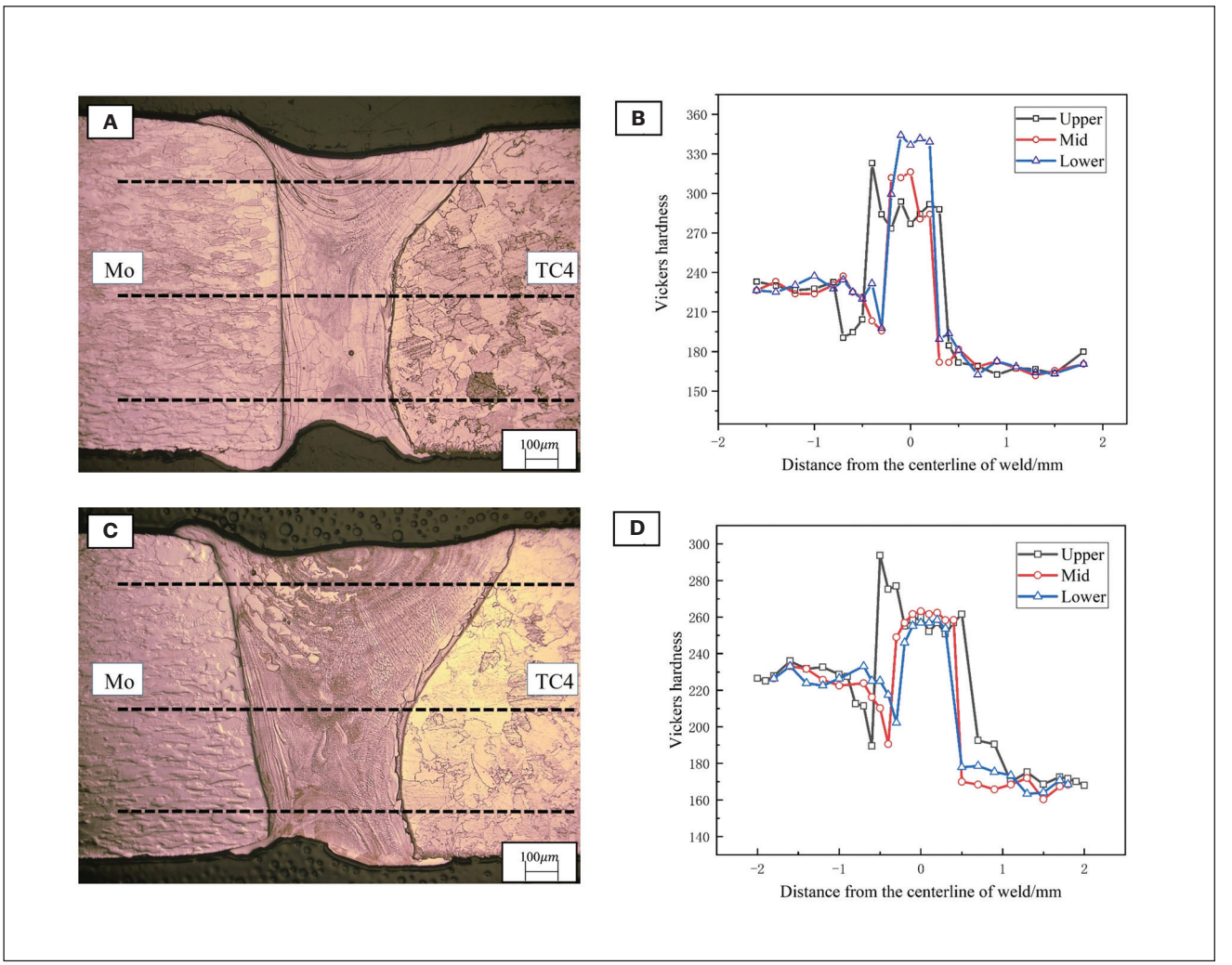

Fig. 10 — A and C — Cross-section morphology of the joint without and with beam oscillation; B and D — hardness distribution curves on cross sections without and with beam oscillation.

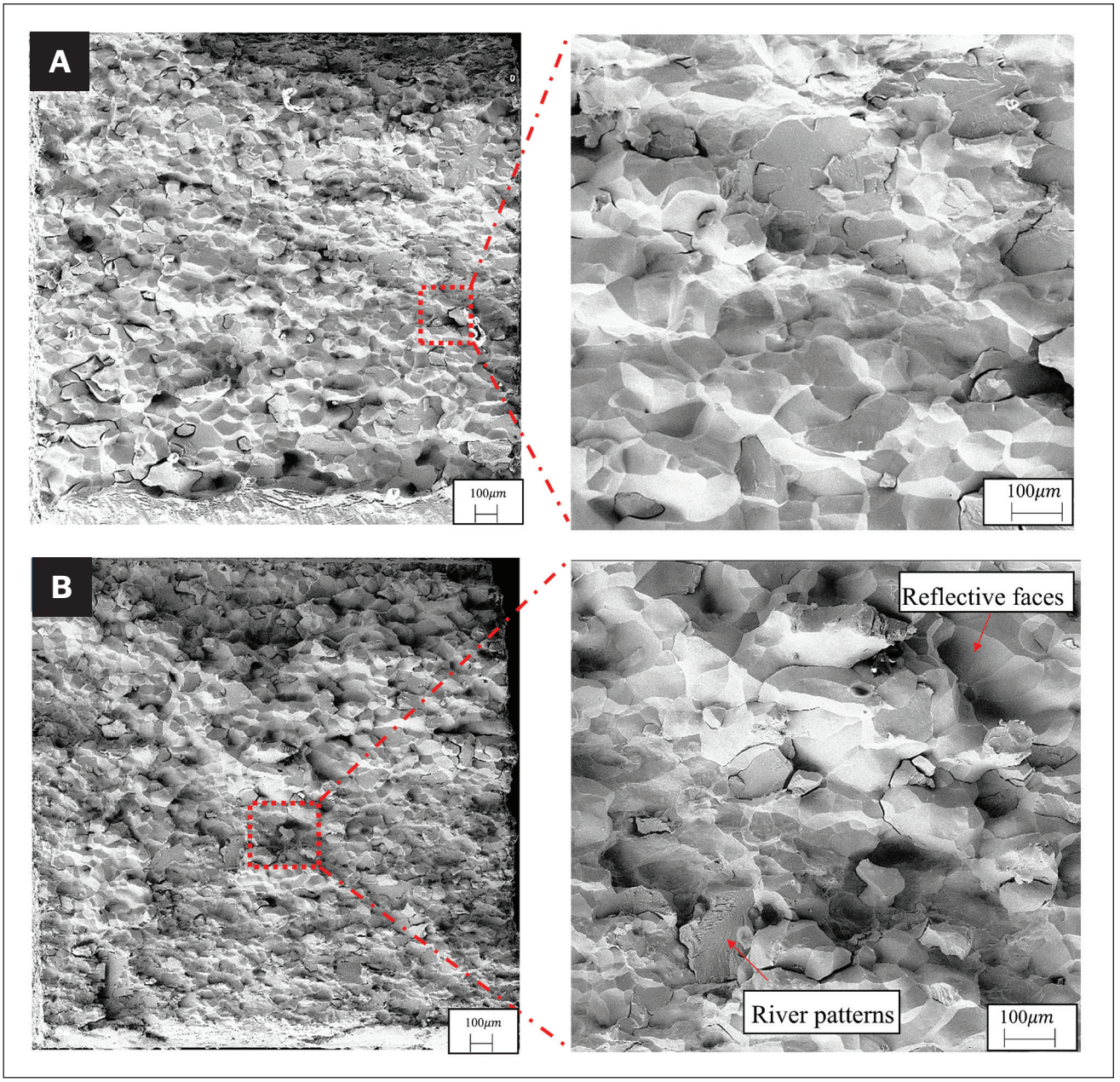

Fig. 11 — Fracture morphology of the joints: A — Without beam oscillation; B — with beam oscillation.

Table 5 — Main Chemical Constituents (at-%) in Fracture Surface

Point	Mo	Ti	V	Al
J	99.4	0.26	0.12	0.04
K	99.72	0.1	0.13	0.05
L	92.00	7.79	0.1	0.11
M	89.25	10.54	0.12	0.09

beam oscillation. The most significant difference was that the fracture surface was much coarser and more uneven. A few river patterns caused by transgranular fracture occurred in the fracture surface. Both fracture surfaces showed typical brittle fractures.

After the element analysis of the fracture surface, it was found that there was almost no Ti element on the fracture surface without beam oscillation, while there was a small amount of Ti element on the upper part of the fracture surface with beam oscillation. This is illustrated in Fig. 12 and Table 5. It shows that the joints fractured at the HAZ of the Mo base metal due to the recrystallization, and the same phenomenon also can be found in the study by Zhang et al. (Ref. 8). However, the recrystallization of HAZ was alleviated by beam

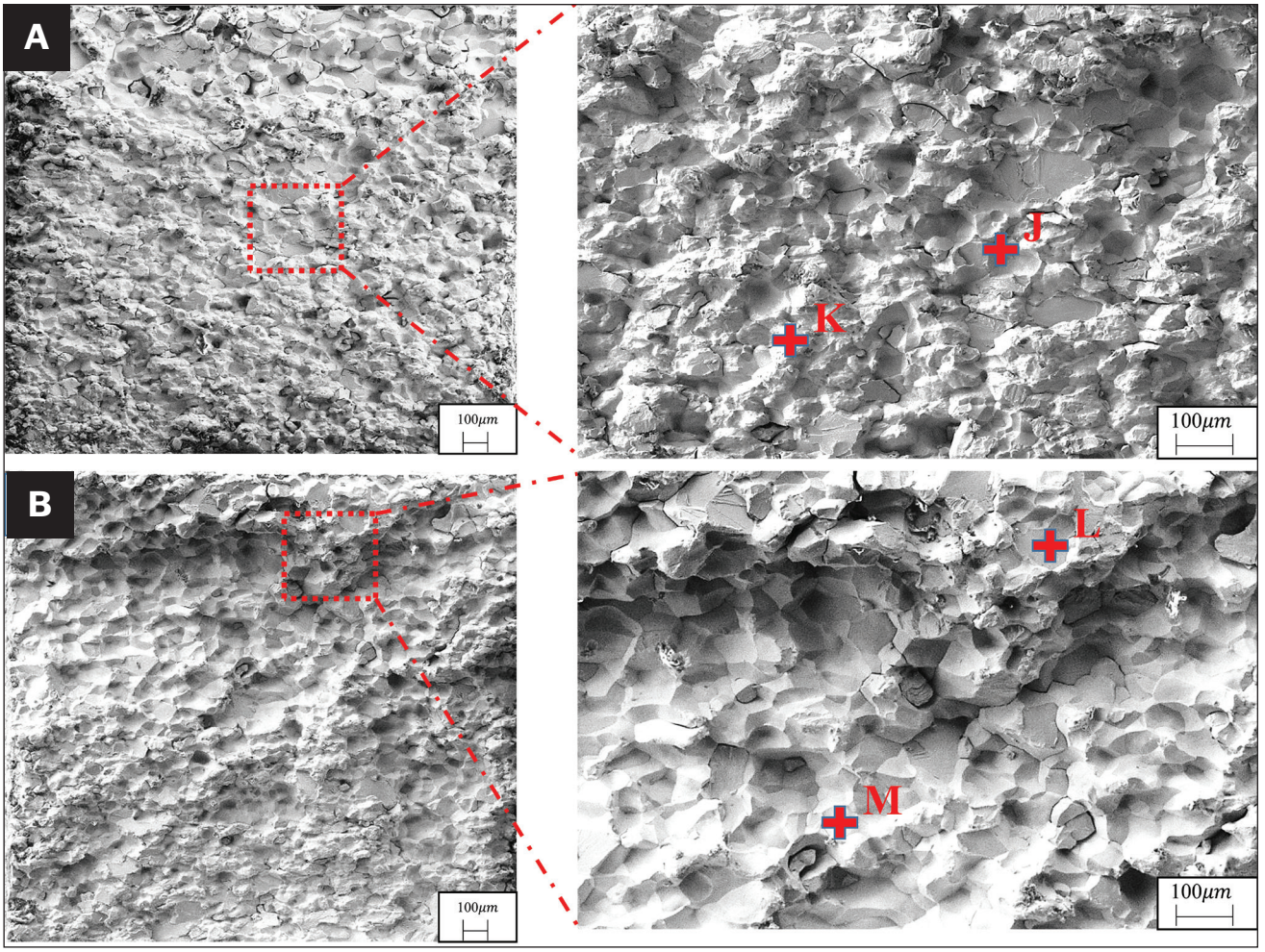

Fig. 12 — Fracture morphology of the joints on the TC4 side: A — Without beam oscillation; B — with beam oscillation.

oscillation, and the properties of the joint were enhanced by the molybdenum-rich solid solution accumulated at the upper part of the weld zone.

Conclusion

The effect of electron beam oscillation welding on the microstructure, element composition, microhardness, and mechanical characteristics of welded joints of pure Mo and TC4 Ti alloys was investigated in this work. The conclusions are summarized as follows.

1. Compared with the joint offset of 0.2 mm to TC4 without beam oscillation, the weld zone of the joint with beam oscillation expanded. The microstructure of the welded joint was altered due to beam oscillation, which refined the grains.

2. A reaction layer was identified on the Mo side in joints welded without beam oscillation. The reaction layer thickness decreased. Due to increased molten Mo in the joint welded with beam oscillation, the reaction layer disappeared in the upper part of the weld zone. The reaction layer consisted of a (Mo, Ti) solid solution.

3. The microhardness distribution of the joint welded with beam oscillation was more consistent, the maximum hardness reduced from 340 HV to 270 HV, and the tensile strength increase from 124 MPa to 204 MPa.

Acknowledgments

The authors acknowledge support from the Key Project of CAS (No. ZDRW-CN-2019-3) and the Youth Innovation Promotion Association, Chinese Academy of Science (No. 2018274). Many thanks to Xiaosong Jiang at Southwest Jiaotong University, Chengdu, Sichuan, China for XRD testing.

References

1. Zhang, Y., Sun, D. Q., Gu, X. Y., and Li, H. M. 2018. Microstructure and mechanical property improvement of dissimilar metal joints for Tc4 Ti alloy to 301l stainless steel. *Journal of Materials Science* 53 (4): 2942-2955. DOI: 10.1007/s10853-017-1708-z

2. Xing, H. R., Hu, P., Zhou, Y. H., Li, S. L., Zuo, Y. G., Cheng, Q., Wang, K. S., et al. 2020. The microstructure and texture evolution of pure molybdenum sheets under various rolling reductions. *Materials Characterization* 165: 11035. DOI: 10.1016/j.matchar.2020.110357

3. Chen, G., Yin, Q., Dong, Z., Zhang, G., Li, Y., Zhao, Y., Zhang, B., and Huang, Y. 2021. Microstructure evolution analysis for the reaction interface between molybdenum and Kovar acquired by

electron beam welding-brazing. *Materials Characterization* 171: 110781. DOI: 10.1016/j.matchar.2020.110781

4. Blank, R., Anglin, S., Beletic, J. W., Bhargava, S., Bradley, R., Cabelli, C. A., Chen, J., et al. 2012. H2rg focal plane array and camera performance update. *Proceedings of SPIE – The International Society for Optical Engineering*, 845310. DOI: 10.1117/12.926752

5. Breniere, X., Rubaldo, L., and Dupont, F. 2014. Sofradir's recent improvements regarding the reliability and performance of HgCdTe ir detectors. *40th Conference on Infrared Technology and Applications*: 836-845. DOI: 10.1117/12.2051705

6. Chen, G., Liu, J., Shu, X., Zhang, B., and Feng, J. 2018. Study on microstructure and performance of molybdenum joint welded by electron beam. *Vacuum* 154: 1-5. DOI: 10.1016/j.vacuum.2018.04.031

7. Ambroziak, A. 2011. Friction welding of molybdenum to molybdenum and to other metals. *International Journal of Refractory Metals & Hard Materials* 29 (4): 462-469. DOI: 10.1016/j.ijrmhm.2011.02.005

8. Zhang, L. J., Lu, G. F., Ning, J., Zhang, L. L., Long, J., and Zhang, G. F. 2018. Influence of beam offset on dissimilar laser welding of molybdenum to titanium. *Materials* 11 (10): 1852. DOI: 10.3390/ma11101852

9. Zhou, X. W., Huang, Y. D., Chen, Y. H., and Peng, P. 2018. Laser joining of Mo and Ta sheets with Ti6al4v or Ni filler. *Optics and Laser Technology* 106: 487-494. DOI: 10.1016/j.optlastec.2018.05.004

10. Yan, F., Qin, Y., Tang, B., Zhou, Y., Gao, Z., Hu, Y., Hu, C., et al. 2022. Effects of beam oscillation on microstructural characteristics and mechanical properties in laser welded steel-copper joints. *Optics and Laser Technology* 148. DOI: 10.1016/j.optlastec.2021.107739

11. Jiang, Z. G., Chen, X., Yu, K., Lei, Z. L., Chen, Y. B., Wu, S. B., and Li, Z. J. 2020. Improving fusion zone microstructure inhomogeneity in dissimilar-metal welding by laser welding with oscillation. *Materials Letters* 261: 126995. DOI: 10.1016/j.matlet.2019.126995

12. Dinda, S. K., Das, D., Mohan, A., Srirangam, P., and Roy, G. G. 2021. Effect of beam oscillation on electron beam butt welded dual-phase (Dp600) steel to 5754 aluminum alloy joints. *Metallurgical and Materials Transactions a-Physical Metallurgy and Materials Science* 52 (5): 1723-1731. DOI: 10.1007/s11661-021-06181-0

13. Torkamany, M. J., Malek Ghaini, F., and Poursalehi, R. 2014. Dissimilar pulsed Nd:YAG laser welding of pure niobium to Ti-6al-4v. *Materials & Design* 53: 915-920. DOI: 10.1016/j.matdes.2013.07.094

14. Chen, G., Yin, Q., Guo, C., Zhang, B., and Feng, J. 2019. Beam deflection effects on the microstructure and defect creation on electron beam welding of molybdenum to Kovar. *Journal of Materials Processing Technology* 267: 280-288. DOI: 10.1016/j.jmatprotec.2018.12.017

15. Oliveira, J. P., Panton, B., Zeng, Z., Andrei, C.M., Zhou, Y., Miranda, R. M., and Braz Fernandes, F. M. 2016. Laser joining of NiTi to Ti6Al4V using a Niobium interlayer. *Acta Materialia* 105: 9-15. DOI; 10.1016/j.actamat.2015.12.021

16. Budkin, Yu V., and Erofeev, V.A. 2011. A physico–mathematical model of the formation of intermetallic compounds in weldbrazing of refractory metals to steel. *Welding International* 25 (8): 633-637. DOI: 10.1080/ 09507116.2011.566736

17. Torkamany, M. J., Malek Ghaini, F., and Poursalehi, R. 2016. An insight to the mechanism of weld penetration in dissimilar pulsed laser welding of niobium and Ti-6al-4v. *Optics and Laser Technology* 79: 100-107. DOI: 10.1016/j.optlastec.2015.11.005

18. Luo, M., Liang, L., Lang, L., Xiao, S., Hu, W., and Deng, H. 2018. Molecular dynamics simulations of the characteristics of Mo/Ti interfaces. *Computational Materials Science* 141: 293-301. DOI: 10.1016/j.commatsci.2017.09.039

19. Barzilai, S., Toher, C., Curtarolo, S., and Levy, O. 2017. Molybdenum-titanium phase diagram evaluated from ab initio calculations. *Physical Review Materials* 1 (2): 023604. DOI: 10.1103/PhysRevMaterials.1.023604

20. Ho, W. F., Ju, C. P. , and Lin, J. H. C. 1999. Structure and properties of cast binary Ti-Mo alloys. *Biomaterials* 20 (22): 2115-2122. DOI: 10.1016/s0142-9612(99)00114-3

XIN-MIN SHI, **DE-FENG MO** (*dfmo@mail.sitp.ac.cn*), **TONG ZHAO**, **YANG ZHANG**, **WEN SUN**, **HAI-MEI GONG**, and **XUE LI** are with the Key Laboratory of Infrared Imaging Materials and Detectors, Shanghai Institute of Technical Physics, Chinese Academy of Sciences, Shanghai, China, and University of Chinese Academy of Sciences, Beijing, China.